Journal of Materials Chemistry A

Accepted Manuscript

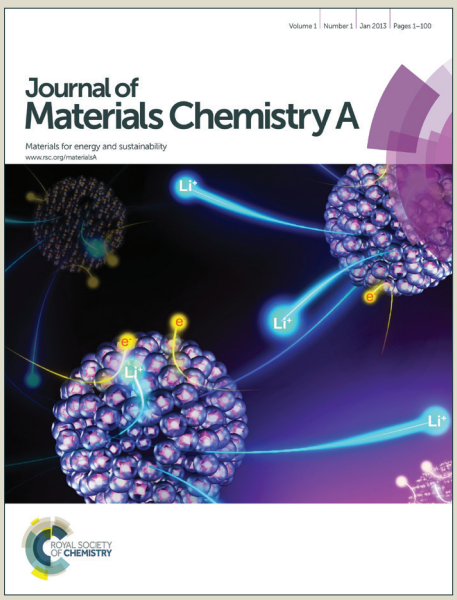

ROYAL SOCIETY OF CHEMISTRY

www.rsc.org/materialsA

Nanoporous Metal Based Flexible Asymmetric Pseudocapacitors

Ying Hou[ab+], Luyang Chen[b+], Pan Liu[b], Jianli Kang[b], Takeshi Fujita[b] and Mingwei Chen[bcd*]

[a] *Key Laboratory of Interface Science and Engineering in Advanced Materials, Taiyuan University of Technology, Ministry of Education, Taiyuan 030024, PR China*

[b] *World Premier International (WPI) Research Center, Advanced Institute for Materials Research, Tohoku University, Sendai 980-8577, Japan*

[c] *CREST, Japan Science and Technology Agency (JST), Saitama 332-0012, Japan*

[d] *State Key Laboratory of Metal Matrix Composites, School of Materials Science and Engineering, Shanghai Jiao Tong University, Shanghai 200030, PR China*

[+]These authors contributed equally to this work.

ABSTRACT

We report a flexible asymmetric supercapacitor assembled by polypyrrole (PPy) and manganese oxide supported by ultrathin three-dimensional nanoporous gold (NPG) electrodes. The highly conductive and free-standing NPG films act as both supports of the active materials and current collectors of the supercapacitor, which evidently enhance the specific capacitance of active materials of both conducting polymer and metal oxide. The high energy density and high power density can be realized from the PPy-NPG//MnO_2-NPG asymmetric supercapacitor because of the wide cell voltage in an aqueous electrolyte and high specific capacitances of both PPy and MnO_2 enhanced by NPG.

Keywords: Nanoporous gold; Asymmetric supercapacitor; Energy density; Capacitance

* Corresponding author. Tel: +81 22 2175963; fax: +81 22 2175955. *E-mail address*: mwchen@wpi-aimr.tohoku.ac.jp

1. Introduction

Along with the increasing demands of green energy resources for environment-friendly applications, electrochemical supercapacitors have attracted much more attentions than before because of the promising higher power density than batteries and higher energy density than conventional dielectric capacitors.[1-2] Supercapacitors have been used as the power supplies in memory backup systems, portable electronics, military devices and hybrid electric vehicles where high power delivery and long cycle-life are required.[3-5] Although the present commercial supercapacitors have a high power density and excellent cycling retention, their energy density, less than 10 Wh/kg, is much lower than those of batteries and fuel cells, which significantly limits their applications when both high energy and power densities are necessary.[1, 6-7] Therefore, improving the energy density of supercapacitors with retained high power density and cycling stability has been the current research topic of electrochemical supercapacitors.

There are two types of supercapacitors according to the mechanisms of charge storage.[1, 8-9] One is electric double-layer capacitors (EDLC) by non-Faradic surface ion adsorption;[5, 10-12] and the other is pseudocapacitors by fast Faradic redox reactions at electrode/electrolyte interfaces. Recently, the pseudocapacitors have attracted considerable attentions because of their much higher specific capacitance than EDLCs.[13-14] Both conducting polymers and transition-metal oxides have been suggested to have high theoretical capacitance and utilized as active electrode materials of pseudocapacitors. However, their poor electric conductivities and narrow working potential windows have been the main factors limiting the practical implementations of the high energy density of the metal oxide and conducting polymer based pseudocapacitors. The energy density (E) of a supercapacitor is determined by the equation: $E = 1/2\ C_s V^2$.[3, 15] Here, C_s is the specific capacitance of the supercapacitor and V is the working potential window of the cell. Therefore, the most effective way to improve the energy density

is to simultaneously increase the operation voltage of the cell and the specific capacitance of the active materials. There are two methods to improve a cell voltage. One is to use non-aqueous electrolytes, such as ionic liquids and organic solutions.[16-18] Although the non-aqueous electrolytes can offer a wide potential window larger than 2 V, the applications are mainly restricted by the dramatic loss of capacitance of active materials because of the poor electrical conductivity of non-aqueous solutions and incomplete surface redox reactions. The other is to employ different electrode materials with complementary working potential windows as negative and positive electrodes, respectively, which can evidently enhance the cell operation voltage in aqueous electrolytes. This new-style supercapacitors, namely asymmetric supercapacitors, have drawn much attention because of its high working voltage. By making use of the two electrodes with the different operating potentials, the cell voltage of the whole device can have a notable improvement in comparison with symmetrical supercapacitors in aqueous electrolytes.[19-21]

Currently, activated carbon (AC) or graphene with electric double capacitance and transition-metal oxides with Faradic capacitance are the most widely used active materials for the asymmetric supercapacitors,[22-25] in which a battery-like Faradic oxide electrode is used as the energy source and a capacitive AC electrode as the power source. For instance, Wu *et al.* developed a high-voltage asymmetric supercapacitor based on graphene as the negative electrode and a MnO_2/graphene composite as the positive electrode.[26] Such graphene-based asymmetric supercapacitor exhibited a wide potential window up to 2 V and a high energy density of 30.4 Wh/kg at the specific capacitance of 30 F/g for the device in a neutral aqueous Na_2SO_4 solution. However, since the device capacitance of the asymmetric supercapacitor depends on the lower capacitance electrode, rather than the higher capacitance one, by the equation: $\frac{1}{C_{\text{Asymmetric Supercapacitor}}} = \frac{1}{C_{\text{Positive Electrode}}} + \frac{1}{C_{\text{Negative Electrode}}}$, the low EDLC capacitance of carbon materials (usually below 100 F/g[27]) limits the overall specific capacitance of the whole

device. Hence, developing new negative materials with a high specific capacitance, appropriate working potential window and low electrical resistance for high power density is the key to achieve a higher specific capacitance and energy density of an asymmetric supercapacitor with a retained high power density.[20, 28, 29]

Recently, three-dimensional nanoporous metals with high electrical conductivity, a large specific surface area and high affinity with active materials have been used as a flexible multifunctional electrode that can obviously enhance the specific capacitance of poor-conductive active materials as supports and effectively reduce the device weight and volume as a current collector simultaneously.[30-34] In this study, we developed a nanoporous metal based asymmetric supercapacitor by using a polypyrrole modified nanoporous gold (PPy-NPG) composite as the negative electrode and manganese dioxide decorated nanoporous gold (MnO_2-NPG) composite as the positive electrode in a neutral aqueous electrolyte. The two electrode materials with comparable high specific capacitance and complementary working potential windows are assembled as an asymmetric supercapacitor with a large operation voltage of 1.8 V. The PPy-NPG//MnO_2-NPG asymmetric supercapacitor shows a high energy density of 86 Wh/kg with the retained power density of 25 kW/kg at the specific device capacitance of 193 F/g, demonstrating the promising applications of the 3D nanoporous metal electrodes in high-performance asymmetric supercapacitors.

2. Experimental Section

2.1. Synthesis of PPy-NPG and MnO_2-NPG hybrid composites

All chemicals in this study were used as received without any further purification. NPG films were fabricated by selectively etching commercial $Au_{35}Ag_{65}$ (at. %) alloy leaves with the size of ~20mm×20mm×100nm in a concentrated HNO_3 solution (wt. 69%) for 8 hours at room temperature. The average pore channel and ligament size of NPG were measured to be

~40 nm. The as-prepared NPG films were rinsed by deionized water (18.2 MΩ·cm) for three times. The NPG film was then fixed to a polyethylene terephthalate (PET) plate as a holder by annealing NPG/PET at the temperature of 80^{o}C for convenient treatment as flexible electrodes.

PPy-NPG composites were prepared by an electrochemical plating method.[35] 1.38 mL Pyrrole (99.0% Wako Pure Chemical Industries) and 5.77 g sodium dodecyl sulfonate (SDS, Kanto Chemical Co., Inc.) were dissolved in 200 mL distilled water to form a 0.1 M solution. The NPG/PET plates were immersed into 0.1 M Pyrrole/SDS electrolyte at the room temperature. The electroplating was performed in a standard three-electrode system with a platinum sheet as the counter electrode, Ag/AgCl as the reference electrode, and an NPG/PET plate as the working electrode. The anodic oxidation synthesis of pyrrole on NPG was conducted by CV with a potential window ranging from -0.2 V to 0.9 V. The MnO_2-NPG composites were also prepared by using an electrochemical plating method.[36, 37] Briefly, the NPG/PET plates were immersed into 0.2 M $Mn(CH_3COO)_2$ and Na_2SO_4 aqueous solution at room temperature. Nanocrystalline MnO_2 was deposited into the nanopore channels of NPG with a constant deposition potential of -0.45 V. The loading amount of MnO_2 was adjusted by the plating time.

The loading amounts of PPy and MnO_2 are calculated from the integration of the plating curves. For PPy, according to Schirmeisen et al.,[38] the deposited PPy mass can be calculated based on the following equation: $m = QM/zF = QM_M/(2+y)F$, where m, Q, y and F are the mass of the deposited PPy, polymerizing charge, a stoichiometric factor evaluating the PPy insertion degree, and the faradic constant, respectively. M_M is the molecular weight of the polymer monomer unit ($M_M = M_{Py}-2$), and M_{Py} is pyrrole molecular weight. The loading amount of the plated MnO_2 was calculated by integrating the total Coulombic charges during the electroplating process, since the current efficiency ($Mn^{2+} + 2H_2O = MnO_2 + 4H^+ + 2e^-$) is nearly 100%.[39]

2.2. Microstructure Characterization

The microstructure and chemical composition of the as-synthesized PPy-NPG and MnO_2-NPG composite electrodes were characterized by a JEOL JIB-4600F scanning electron microscope (SEM) equipped with an Oxford energy dispersive X-ray spectroscopy (EDS) and a JEOL JEM-2100F transmission electron microscope (TEM) equipped with double spherical aberration correctors. The chemical state of the electroplated MnO_2 was investigated by X-ray photoelectron spectroscopy (XPS, AxIS-ULTRA-DLD) with Al Kα (mono) anode at energy of 150 W in a vacuum of 10^{-7} Pa.

2.3. Assembly of PPy-NPG//MnO_2-NPG asymmetric supercapacitors

Two-electrode asymmetric supercapacitor devices were constructed with one PPy-NPG/PET plate as the negative electrode, one MnO_2-NPG/PET plate as the positive electrode and a thin cotton paper (~40 μm in thickness, Bemliese™) as the separator (Fig. 2a). For comparison, the PPy-NPG//PPy-NPG and MnO_2-NPG//MnO_2-NPG two-electrode symmetric supercapacitors were also assembled with a cotton paper as the separator, respectively.

2.4. Electrochemical measurements

The capacitance measurements of the PPy-NPG and MnO_2-NPG symmetric supercapacitors and PPy-NPG//MnO_2-NPG asymmetric supercapacitors were investigated by a classic two-electrode electrochemical system (Ivium Technology). A neutral electrolyte, 1 M $LiClO_4$ aqueous solution, was used as the electrolyte for the supercapacitors.

3. Results and Discussion

Fig. 1a and 1c show the SEM and bright-field TEM images of the PPy-NPG hybrid electrode with an open nanoporous structure. The PPy coating forms a core-shell structure in which the conducting polymer displays bright contrast as the shell that uniformly covers the internal surfaces of the metal ligaments that have the dark contrast. High-resolution TEM

(HRTEM) image (Fig. 1e) proves the well-bonded PPy/Au interface and the deposited PPy has an amorphous structure without any well-defined periodic lattice. Fig. 1b, d and f elucidate the microstructure of the MnO_2-NPG composite. The MnO_2 layer uniformly distributes on the NPG film as shown in the SEM image (Fig. 1b). The bright-field TEM reveals that the MnO_2 coating has a nanocrystalline structure and forms on the internal surface of gold ligaments of NPG (Fig. 1d). The hybrid structure is readily identified by contrast difference between the bright metal oxide and the dark gold skeleton. The well-defined periodic lattices with random orientations of MnO_2 nanocrystals can be seen from the HRTEM image (Fig. 1f), confirming the nanocrystalline nature of the electrodeposited MnO_2. XPS measurements of the electroplated MnO_2 (Fig. S1) show that the mean valence of Mn, calculated from the areas under each deconvulated curves of Mn 2p orbits, is ~2.98, indicating mixed bonding states of Mn and defective structure of the electrodeposited MnO_2.[36]

The assembly schematic and photograph of the PPy-NPG//MnO_2-NPG two-electrode flexible asymmetric supercapacitor are shown in Fig. 2a and 2b. The cyclic voltammetry (CV) curves of the PPy-NPG and MnO_2-NPG electrodes in a 1 M $LiClO_4$ electrolyte are shown in Fig. 2c. The potential window of the PPy-NPG electrode spans from -0.5 V to 0.5 V while that of the MnO_2-NPG electrode between 0 V and 0.8 V. As for an asymmetric supercapacitor, the charge balance of two electrodes should follow the relationship of $q_+ = q_-$, which is strongly dependent on the mass of active materials in the anode and cathode. The mass balance can be decided by the equation: $m_+/m_- = (C_- \times \Delta E_-)/(C_+ \times \Delta E_+)$. Following this equation, the m_+/m_- should be ~1.17. Obviously, the loading amounts of PPy and MnO_2 can be adjusted by the plating time. In the study, the PPy-NPG and MnO_2-NPG composites with different plating time were prepared to optimize the performance of the asymmetric supercapacitor. Fig. S2a and S2b shows the specific capacitance of the PPy-NPG//MnO_2-NPG asymmetric supercapacitor with different PPy plating cycle of 1, 3, and 5 cycles. At the same

current density of 1 A/g, the highest specific capacitance is the 1-cycle sample, which suggests the smaller PPy loading amount give better capacitance. Moreover, the effect of MnO_2 loading amount to the electrochemical properties of the asymmetric supercapacitor were also studied. Fig. S2c and S2d show the specific capacitance of PPy-NPG//MnO_2-NPG asymmetric supercapacitor with different MnO_2 plating time of 7.5, 10, and 12.5 min, respectively. The 7.5-min sample shows the best performance. Therefore, the 1-cycle PPy-NPG and the 7.5-min MnO_2-NPG were chosen to fabricate the PPy-NPG//MnO_2-NPG asymmetric supercapacitor. The loading amount of PPy and MnO_2 are ~60 μg and 50 μg, respectively. Meanwhile, the active material loading amount of asymmetric supercapacitor is the total active material mass of both electrodes.

Fig. 2d exhibits the CV curves of optimized PPy-NPG//MnO_2-NPG asymmetric supercapacitors with different potential windows. The maximum potential window can achieved from 0 to 1.8 V. Nevertheless, when the device was operated at voltages higher than 1.8 V, the current density increases rapidly and results in an irreversible reaction. Therefore, we chose a potential window of 1.8 V in 1 M $LiClO_4$ electrolyte to further study the entire electrochemical performance of the optimized asymmetric supercapacitor. It is worth to note that the asymmetric supercapacitor was firstly activated in the electrolyte shown in Fig. 2d. The redox peaks exhibited the incipient activation of both PPy-NPG and MnO_2-NPG electrodes in $LiClO_4$ aqueous solution. After several cycles, the asymmetric supercapacitor becomes stable and the CV curve exhibits quasi-rectangle shape shown in Fig. 3a, which is similar with the CV curves of individual electrode.

Fig. 3a reveals the CV curves of the PPy-NPG//MnO_2-NPG supercapacitor in a 1 M $LiClO_4$ electrolyte at the scan rates of 10, 50, 100, 200 and 300 mV/s. The CV curves present a good symmetric shape during the forward and backward scans, suggesting the excellent capacitive ability of the asymmetric supercapacitor. On the basis of the CV curves, the

specific capacitances of the PPy-NPG//MnO_2-NPG asymmetric supercapacitor, PPy-NPG//PPy-NPG symmetric supercapacitor and MnO_2-NPG//MnO_2-NPG symmetric supercapacitor are presented in Fig. 3b. The total mass of active materials on the two electrodes of the supercapacitors was used to calculate the specific capacitances. The specific capacitance of the asymmetric supercapacitor is between those of MnO_2-NPG//MnO_2-NPG and PPy-NPG//PPy-NPG symmetric supercapacitor, which are close to each other. As the scan rate increases from 10 to 1000 mV/s, the specific capacitance of the PPy-NPG//MnO_2-NPG supercapacitor gradually reduces from ~195 F/g to ~150 F/g, showing an excellent high-rate performance.

Representative galvanostatic charge/discharge curves of the PPy-NPG//MnO_2-NPG supercapacitor as the function of current densities are illustrated in Fig. 3c. The discharge time of the supercapacitor decreases with the current density increasing. The specific capacitance of the asymmetric supercapacitor at different current densities is calculated according to the charge/discharge curves by the formula $C_s = i/[-(\triangle E/\triangle t)m]$, where i is the applied current; $-\triangle E/\triangle t$, the slope of the discharge curve after the voltage drop at the beginning of each discharge ($\triangle E_{IR}$); and m is the mass of total active materials of the two electrodes. Fig. 3d elucidates the specific capacitance of the asymmetric supercapacitor compared with other two symmetric supercapacitors. As the discharge current density increases from 2 A/g to 20 A/g, the specific capacitance of the PPy-NPG//MnO_2-NPG supercapacitor decreases from ~193 F/g to ~163 F/g in the neutral electrolyte. The high specific capacitance results from the matched capacitances of the PPy-NPG and MnO_2-NPG electrodes which are enhanced by the highly conductive NPG with a large surface area.[30, 35] It is worth noting that the specific capacitance of bare NPG is less than 1% of those of PPy and MnO_2.[40] Therefore, the contribution of NPG can be neglected in the total capacitance of MnO_2//PPy asymmetric supercapacitor.

The internal resistance (R) of the supercapacitor cells is determined by the initial voltage drop (ΔV_{IR}) and discharge current density, i.e., $R = \Delta V_{IR}/I$. Fig. S3 exhibits the internal resistances of the PPy-NPG//MnO_2-NPG supercapacitor, MnO_2-NPG//MnO_2-NPG supercapacitor, and PPy-NPG//PPy-NPG supercapacitor in a 1 M $LiClO_4$ electrolyte at the discharge current densities of 5, 10, and 16 A/g, respectively. The internal resistance of PPy-NPG//MnO_2-NPG supercapacitor is ~24 Ω, while those of the MnO_2-NPG//MnO_2-NPG supercapacitor and PPy-NPG//PPy-NPG supercapacitor are ~23 Ω and ~26 Ω, respectively. The higher capacitance, wide potential window and lower internal resistance give rise to the higher energy density (E) and power density (P) since $E = 0.5CV^2$ and $P = V^2/(4Rm)$, where V is the cutoff voltage, C is the measured device capacitance, and $R = \Delta V_{IR}/(2i)$ with ΔV_{IR} being the voltage drop between the first two points in the voltage drop at its top cutoff. For comparison, the Ragone plots of the PPy-NPG//MnO_2-NPG supercapacitor, MnO_2-NPG//MnO_2-NPG supercapacitor and PPy-NPG//PPy-NPG supercapacitor in a neutral electrolyte are illustrated in Fig. 4a. The energy density of 86 Wh/kg along with the power density of 25 kW/kg of the PPy-NPG//MnO_2-NPG supercapacitor are much higher than those of the MnO_2-NPG//MnO_2-NPG and PPy-NPG//PPy-NPG supercapacitors. Meanwhile, Table 1 shows the higher energy and power density of PPy-NPG//MnO_2-NPG supercapacitor compared to other previously reported asymmetric supercapacitors.[19, 41-44] Although the Ragone plots only represent the energy and power densities of the active materials, not the entire cells, it unambiguously demonstrates that the 3D nanoporous metal electrodes can significantly improve the capacitive performance of the asymmetric supercapacitor by enhancing the specific capacitance of active materials and lessening the internal resistance of the device. Fig. 4b shows the cycling stability of the PPy-NPG//MnO_2-NPG asymmetric supercapacitor in a 1 M $LiClO_4$ electrolyte at the scan rate of 100mV/s. After 2000 cycles, the

specific capacitance can retain as high as ~85 % of the initial value, verifying the good cycling retention of the asymmetric supercapacitor.

4. Conclusion

In summary, we have successfully developed a PPy-NPG//MnO_2-NPG flexible asymmetric supercapacitor by using the highly conductive 3D nanoporous metal as the electrodes and current collectors to support high-capacitance but poor-conductivity PPy and MnO_2. The asymmetric supercapacitor shows a wide operation potential window of 1.8 V, the high specific capacitance of ~193 F/g and a low internal resistance of ~24 Ω, leading to the realization of both high energy and power density from a single supercapacitor cell. This study may pave a new way to develop nanoporous metal based asymmetric supercapacitors for high energy and high power applications.

Acknowledgements

This research was sponsored by JST-CREST "Phase Interface Science for Highly Efficient Energy Utilization" project; and World Premier International (WPI) Research Center Initiative for Atoms, Molecules and Materials, MEXT, Japan.

Notes and references

1 B. E. Conway, *Electrochemical Supercapacitors*. Kluwer Academic: New York, 1999.

2 C. Liu, F. Li, L.-P. Ma, H.-M. Cheng, *Adv. Mater.,* 2010, **22**, E28-E62.

3 P. Simon, Y. Gogotsi, *Nat. Mater,* 2008, **7**, 845-854.

4 T.-Y. Wei, C.-H. Chen, H.-C. Chien, S.-Y. Lu, C.-C. Hu, *Adv. Mater.,* 2010, **22**, 347-351.

5 J. R. Miller, P. Simon, *Science,* 2008, **321**, 651-652.

6 C. F. Zhou, S. Kumar, C. D. Doyle, J. M. Tour, *Chem. Mater.,* 2005, **17**, 1997-2002.

7 A. L. M. Reddy, M. M. Shaijumon, S. R. Gowda, P. M. Ajayan, *J. Phys. Chem. C,* 2009, **114**, 658-663.

8 A. Burke, *J. Power Sources,* 2000, **91**, 37-50.

9 A. S. Arico, P. Bruce, B. Scrosati, J.-M. Tarascon, W. van Schalkwijk, *Nat. Mater,* 2005, **4**, 366-377.

10 X. Y. Lang, H. T. Yuan, Y. Iwasa, M. W. Chen, *Scripta Mater.,* 2011, **64**, 923-926.

11 Z. Q. Niu, W. Y. Zhou, J. Chen, G. X. Feng, H. Li, W. J. Ma, J. Z. Li, H. B. Dong, Y. Ren, D. Zhao, S. S. Xie, *Energy & Environ. Sci.,* 2011, **4**, 1440-1446.

12 M. Cortie, A. Maaroof, G. Smith, *Gold Bull.,* 2005, **38**, 14-22.

13 J. T. Zhang, J. W. Jiang, H. L. Li, X. S. Zhao, *Energy & Environ. Sci.,* 2011, **4**, 4009-4015.

14 G. Milczarek, O. Inganäs, *Science,* 2012, **335**, 1468-1471.

15 J.-K. Chang, M.-T. Lee, C.-W. Cheng, W.-T. Tsai, M.-J. Deng, Y.-C. Hsieh, I. W. Sun, *J. Mater. Chem.,* 2009, **19**, 3732-3738.

16 T. Abdallah, D. Lemordant, B. Claude-Montigny, *J. Power Sources,* 2012, **201**, 353-359.

17 A. Balducci, R. Dugas, P. L. Taberna, P. Simon, D. Plée, M. Mastragostino, S. Passerini, *J. Power Sources,* 2007, **165**, 922-927.

18 J. S. Shaikh, R. C. Pawar, R. S. Devan, Y. R. Ma, P. P. Salvi, S. S. Kolekar, P. S. Patil, *Electrochimica Acta,* 2011, **56**, 2127-2134.

19 Y. G. Wang, Y. Y. Xia, *Electrochem. Comm.*, 2005, **7**, 1138-1142.

20 L. Y. Chen, Y. Hou, J. L. Kang, M. W. Chen, *J. Mater. Chem. A, 2014* **DOI:** 10.1039/C4TA00965G.

21 Y.-P. Lin, N.-L. Wu, *J. Power Sources,* 2011, **196**, 851-854.

22 Z. J. Fan, J. Yan, T. Wei, L. J. Zhi, G. Q. Ning, T. Y. Li, F. Wei, *Adv. Funct. Mater.,* 2011, **21**, 2366-2375.

23 P.-C. Chen, G. Shen, Y. Shi, H. Chen, C. Zhou, *ACS Nano,* 2010, **4**, 4403-4411.

24 L. H. Bao, X. D. Li, *Adv. Mater.*, 2012, **24**, 3246-3252.

25 A. Sumboja, C. Y. Foo, X. Wang, P. S. Lee, *Adv. Mater.*, 2013, **25**, 2809-2815.

26 Z.-S. Wu, W. Ren, D.-W. Wang, F. Li, B. Liu, H.-M. Cheng, *ACS Nano,* 2010, **4**, 5835-5842.

27 K. H. An, W. S. Kim, Y. S. Park, Y. C. Choi, S. M. Lee, D. C. Chung, D. J. Bae, S. C. Lim, Y. H. Lee, *Adv. Mater.,* 2001, **13**, 497-500.

28 X. H. Lu, M. H. Yu, G. M. Wang, T. Zhai, S. L. Xie, Y. C. Ling, Y. X. Tong, Y. Li, *Adv. Mater.*, 2013, **25**, 267-272.

29 X. Xiao, T. P. Ding, L. Y. Yuan, Y. Q. Shen, Q. Zhong, X. H. Zhang, Y. Z. Cao, B. Hu, T. Zhai, L. Gong, J. Chen, Y. X. Tong, J. Zhou, Z. L. Wang, *Adv. Energy Mater.*, 2012, **2**, 1328-1332.

30 X. Y. Lang, A. Hirata, T. Fujita, M. W. Chen, *Nature Nanotech.,* 2011, **6**, 232-236.

31 F. H. Meng, Y. Ding, *Adv. Mater.,* 2011, **23**, 4098-4102.

32 X. Y. Lang, L. Zhang, T. Fujita, Y. Ding, M. W. Chen, *J. Power Sources,* 2012, **197**, 325-329.

33 L. Y. Chen, Y. Hou, J. L. Kang, A. Hirata, T. Fujita, M. W. Chen, *Adv. Energy Mater.,* 2013, **3**, 851-856.

34 J. L. Kang, A. Hirata, H. J. Qiu, L.Y. Chen, X. B. Ge, T. Fujita, M. W. Chen, *Adv. Mater.,* 2014, **26**,269-272.

35 Y. Hou, L. Y. Chen, L. Zhang, J. L. Kang, T. Fujita, J. H. Jiang, M. W. Chen, *J. Power Sources,* 2013, **225**, 304-310.

36 J. L. Kang, A. Hirata, L. J. Kang, X. M. Zhang, Y. Hou, L. Y. Chen, C. Li, T. Fujita, K. Akagi, M. W. Chen, *Angew. Chem. Int. Ed.*, 2013, **52**, 1664-1667.

37 L. Y. Chen, J. L. Kang, Y. Hou, P. Liu, T. Fujita, A. Hirata, M. W. Chen, *J. Mater. Chem. A*, 2013, **1**, 9202-9207.

38 M. Schirmeisen, F. Beck, *J. Appl. Electrochem.*, 1989, **19**, 401-409.

39 M. Nakayama, T. Kanaya, R. Inoue, *Electrochem. Commun.*, 2007, **9**, 1154-1158.

40 X. Y. Lang, H. T. Yuan, Y. Iwasa, M. W. Chen, *Scripta Mater.* 2011, **64**, 923-926.

41 Z. S. Wu, W. C. Ren, D. W. Wang, F. Li, B. L. Liu, H. M. Cheng, *ACS Nano*, 2010, **4**, 5835-5842.

42 H. L. Wang, Y. Y. Liang, T. Mirfakhrai, Z, Chen, H. S. Casalongue, H. J. Dai, *Nano Res.*, 2011, **4**, 729-736.

43 Z. Tang, C. -H. Tang and H. Gong, *Adv. Funct. Mater.*, 2012, **22**, 1272-1278.

44 L. J. Deng, G. Zhu, J. F. Wang, L. P. Kang, Z. H. Liu, Z. P. Yang, Z. L. Wang, *J. Power sources*, 2011, **196**, 10782-10787.

Figures and Captions

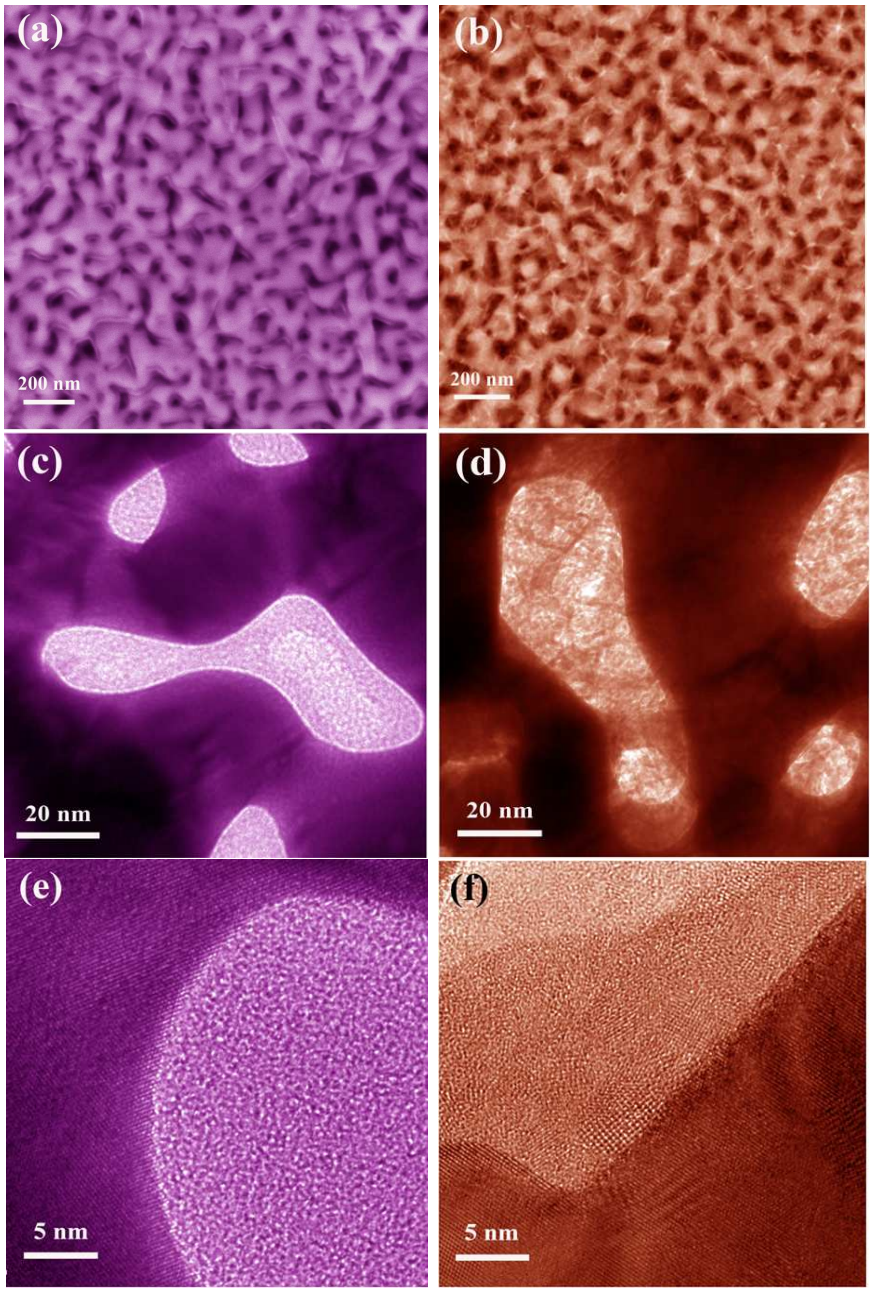

Fig. 1. Representative SEM and TEM images of (a, c) PPy-NPG composite electroplated for 1 cycle; and (b, d) MnO_2-NPG composite electroplated for 7.5 min. HRTEM images showing the interfacial structures of (e) PPy-NPG composite; and (f) MnO_2-NPG composite.

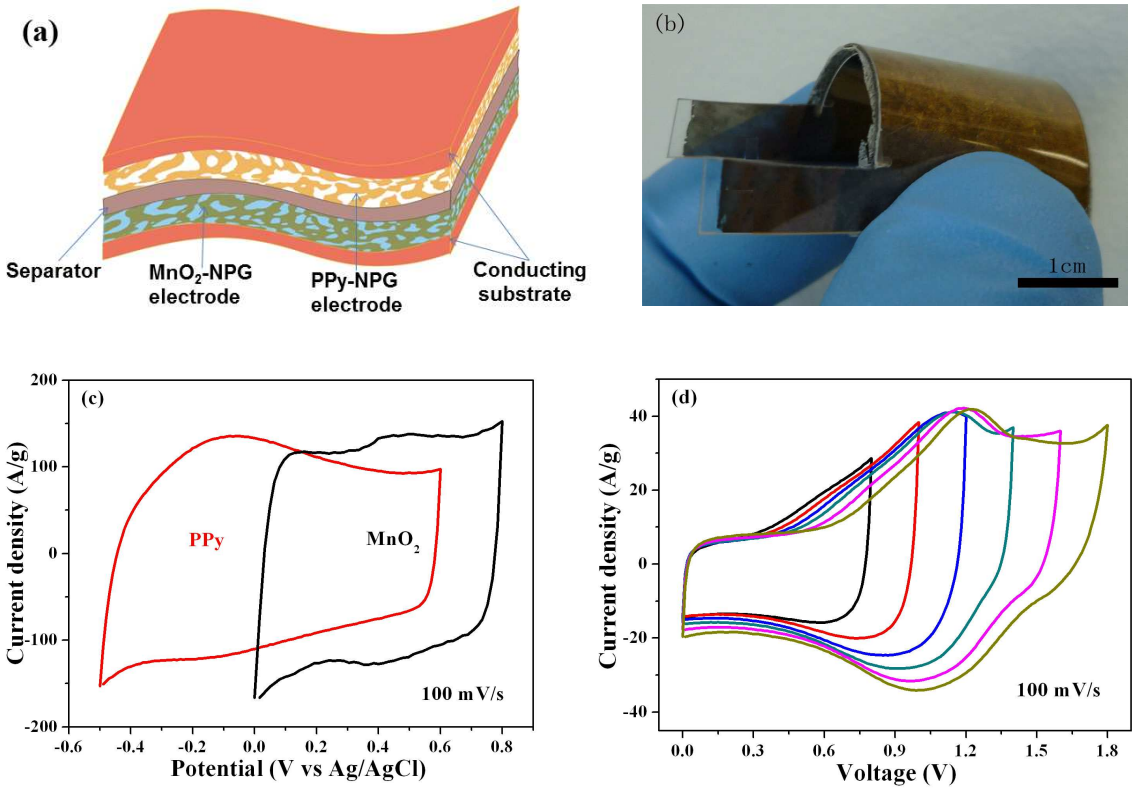

Fig. 2. (a) Assembly schematic of the PPy-NPG//MnO_2-NPG asymmetric supercapacitor. (b) Photograph of a PPy-NPG//MnO_2-NPG asymmetric supercapacitor. (c) CV curves of PPy-NPG and MnO_2-NPG electrodes in different potential windows, which were measured by using a three-electrode system in a 1M $LiClO_4$ aqueous solution. (d) CV curves of the optimized PPy-NPG//MnO_2-NPG asymmetric supercapacitor measured in different potential windows in a 1M $LiClO_4$ aqueous solution. Scan rate: 100 mV/s.

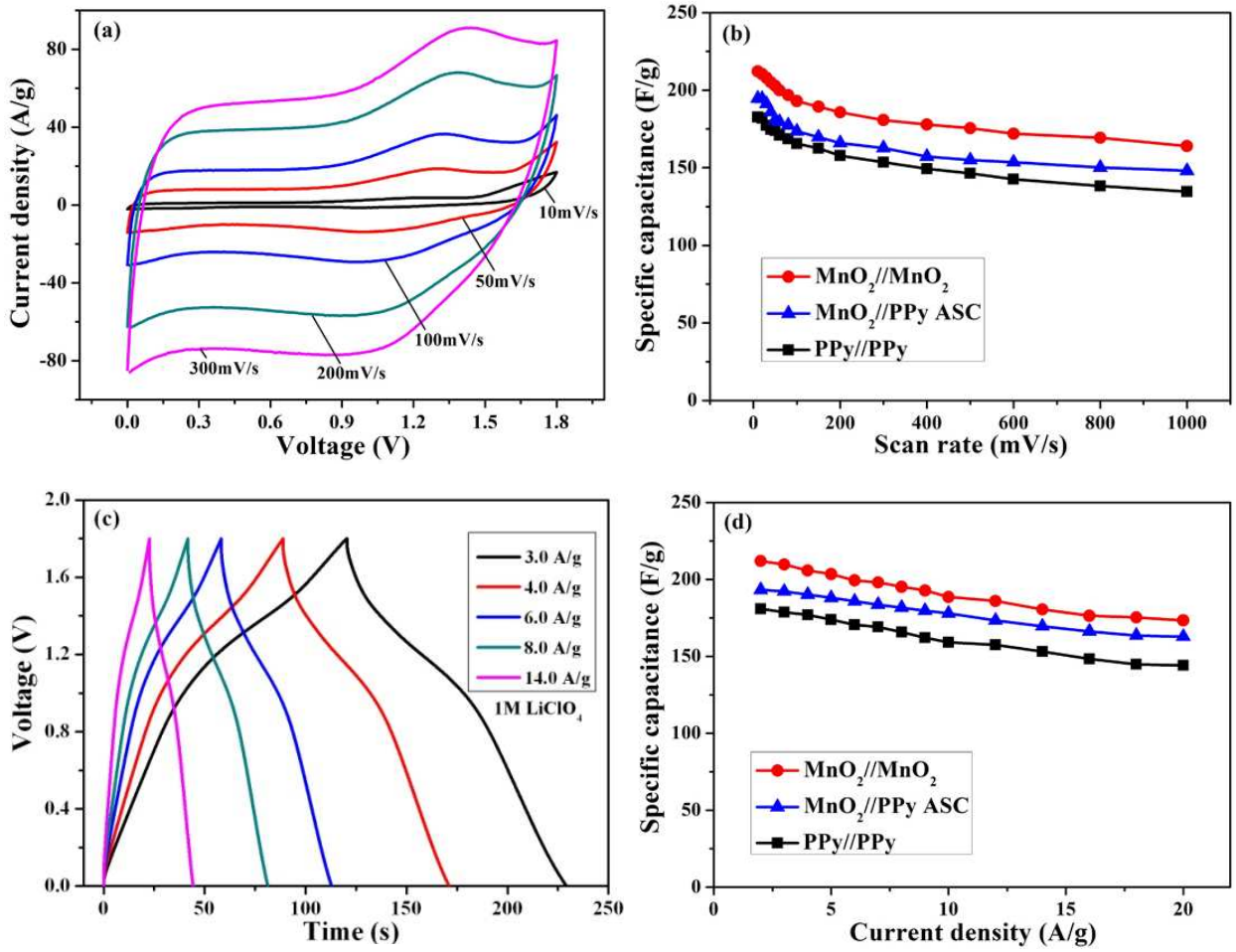

Fig. 3. (a) CV curves of the optimized PPy-NPG//MnO_2-NPG asymmetric supercapacitor at different scan rates in a 1M $LiClO_4$ aqueous solution. (b) Specific capacitance at different scan rates of PPy-NPG//MnO_2-NPG asymmetric supercapacitor, PPy-NPG//PPy-NPG symmetric supercapacitor and MnO_2-NPG//MnO_2-NPG symmetric supercapacitor. (c) Charge/discharge curves for the optimized PPy-NPG//MnO_2-NPG asymmetric supercapacitor measured at different current densities in a 1M $LiClO_4$ aqueous solution. (d) Comparison of specific capacitance of PPy-NPG//MnO_2-NPG asymmetric supercapacitor, PPy-NPG//PPy-NPG symmetric supercapacitor and MnO_2-NPG//MnO_2-NPG symmetric supercapacitor at different current densities.

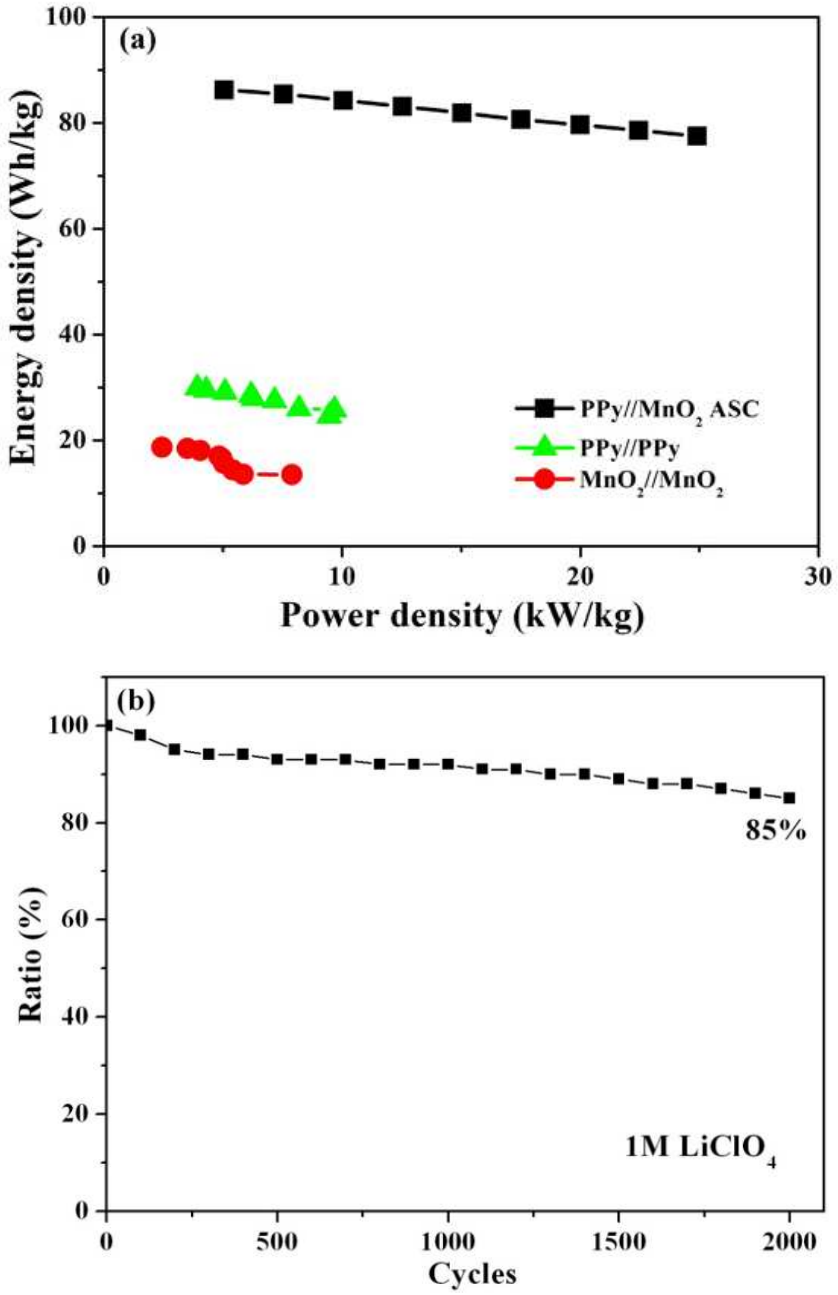

Fig. 4. (a) Ragone plots showing the energy and power densities of the active materials in the PPy-NPG//MnO_2-NPG asymmetric supercapacitor, PPy-NPG//PPy-NPG symmetric supercapacitor and MnO_2-NPG//MnO_2-NPG symmetric supercapacitor. (b) Capacitance retention ratio of the PPy-NPG//MnO_2-NPG asymmetric supercapacitor from the 1st to the 2000th cycle at a scan rate of 100 mV/s in 1M $LiClO_4$.

Table 1. Comparison of E and P with other previously reported asymmetrical supercapacitors.

Electrodes	Energy density (Wh/kg)	Power density (kW/kg)	Ref.
PPy-NPG//MnO_2-NPG	86	25	This work
Activated carbon//$LiMn_2O_4$	35	0.1	[19]
MnO_2 nanowire//Graphene	30.4	5	[41]
$Ni(OH)_2$/graphene//RuO_2/graphene	48	21	[42]
$Ni(OH)_2$//CNT	50.6	2	[43]
Graphene MnO_2//Graphene	10.03	2.53	[44]

Table of contents

Nanoporous Metal Based Flexible Asymmetric Pseudocapacitors

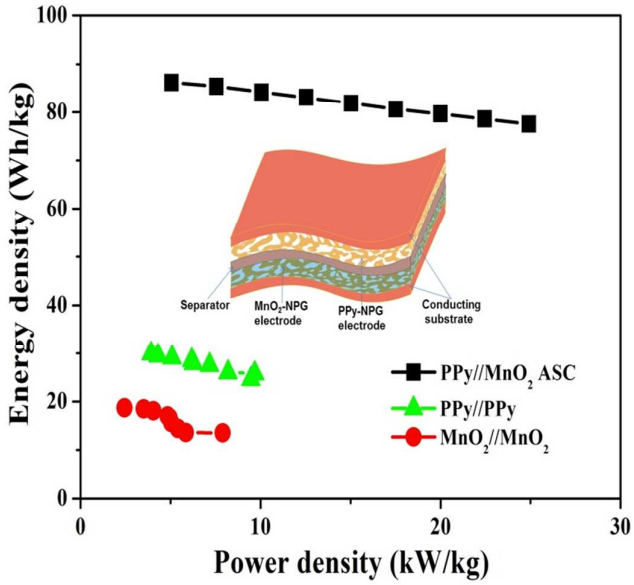

Nanoporous gold dramatically enhances specific capacitances of PPy and MnO_2, resulting in ultrahigh energy density and power density of PPy-NPG//MnO_2-NPG asymmetric supercapacitor with wide potential window.